The Imaging X-ray Polarimetry Explorer (IXPE)

Martin C. Weisskopf [1,*1], Brian Ramsey[1], Stephen O'Dell[1], Allyn Tennant[1], Ronald Elsner[1], Paolo Soffitta[1], Ronaldo Bellazzini[1], Enrico Costa[1], Jeffery Kolodziejczak[1], Victoria Kaspi[3], Fabio Mulieri[2], Herman Marshall[4], Giorgio Matt[5], Roger Romani[6], on behalf of the entire IXPE Team

[1] NASA/Marshall Space Flight Center, ZP12, 320 Sparkman Drive, Huntsville AL USA 35805.
[2] IAPS/INAF, Rome Italy
[3] McGill University, Montreal, Canada
[4] Massachusetts Institute of Technology, Cambridge, MA USA
[5] University Roma Tre, Rome Italy
[6] Stanford University

ABSTRACT

The Imaging X-ray Polarimetry Explorer (*IXPE*) expands observation space by simultaneously adding polarization measurements to the array of source properties currently measured (energy, time, and location). *IXPE* will thus open new dimensions for understanding how X-ray emission is produced in astrophysical objects, especially systems under extreme physical conditions—such as neutron stars and black holes. Polarization singularly probes physical anisotropies—ordered magnetic fields, aspheric matter distributions, or general relativistic coupling to black-hole spin—that are not otherwise measurable. Hence, *IXPE* complements all other investigations in high-energy astrophysics by adding important and relatively unexplored information to the parameter space for studying cosmic X-ray sources and processes, as well as for using extreme astrophysical environments as laboratories for fundamental physics.

Keywords: X-ray astronomy, X-ray polarimetry, X-ray imaging

1. INTRODUCTION

IXPE brings together an international collaboration for the purpose of flying an imaging X-ray polarimeter on one of NASA's small explorers. *IXPE* will conduct X-ray polarimetry for several categories of cosmic X-ray sources—from neutron stars and stellar-mass black holes, to supernova remnants, to active galactic nuclei—that are likely to be X-ray polarized. For the brighter extended sources—Pulsar Wind Nebulae (PWNe), Supernova Remnants (SNR), and large-scale jets in Active Galactic Nuclei (AGN)—*IXPE* will perform X-ray polarimetric imaging.

Only a few previous experiments all involving the *IXPE* PI have conducted unambiguous X-ray polarimetry of cosmic sources. Several rocket observations measured X-ray linear polarization from the Crab Nebula [1]. The Orbiting Solar Observatory (*OSO-8*) X-ray polarimeter confirmed [2,3] this result at high significance ($\Pi = 19.2\% \pm 1.0\%$), thus proving the synchrotron origin of X-radiation from this pulsar wind nebula. Due to limited observing time, the *OSO-8* X-ray polarimeter obtained useful upper limits for just a few other bright galactic X-ray sources [4,5]. At soft-γ-ray energies, un-polarization-calibrated detectors serving as Compton polarimeters [6,7] reported linear polarization from a few very bright sources—the Crab Nebula [8], Cygnus X-1 [9], and γ-ray bursts (GRBs) [10,11,12] although none of these latter results are completely unambiguous.

IXPE improves previous sensitivity over the OSO-8 polarimeter by two orders of magnitude and uniquely provides imaging capability to reach new science objectives. IXPE combines these attributes with simultaneous spectral and temporal measurements. Measurements with IXPE will provide previously unobtainable data to understand the nature of X-ray sources, helping to answer key questions such as the following:

[1] Martin.C.Weisskopf@nasa.gov; Phone 1 256 961-7798; FAX 1 257 961-7522

Space Telescopes and Instrumentation 2016: Ultraviolet to Gamma Ray, edited by Jan-Willem A. den Herder, Tadayuki Takahashi, Marshall Bautz, Proc. of SPIE Vol. 9905, 990517 · © 2016 SPIE · CCC code: 0277-786X/16/$18 · doi: 10.1117/12.2235240

- What is the geometry and the emission mechanism(s) of Active Galactic Nuclei and microquasars?
- What is the geometry and strength of the magnetic field in magnetars?
- What is the geometry and origin of the X-radiation from radio pulsars?
- How are particles accelerated in Pulsar Wind Nebulae?

2. TECHNICAL OVERVIEW

IXPE is comprised of three X-ray telescopes with identical mirror modules and identical polarization-sensitive imaging detectors at their focus. The mirror modules are based on nickel-cobalt replicated optics pioneered by Marshall Space Flight Center. MSFC recently delivered 8 fully flight-qualified mirror modules to Russia as part of another (*ART-XC*) flight program. The X-ray detectors, invented and developed by the *IXPE* Italian partners, are especially well-suited for polarimetry and a prototype has undergone full qualification including life-time testing. Based on proportional counters with highly-pixelated readouts, these detectors offer low gain (not susceptible to sparking) and two-dimensional symmetry (nearly unsusceptible to systematic effects).

The basic scientific operating parameters are as follows:

- 2–8 keV energy range
- Proportional counter energy resolution
- <100 μ-sec time resolution
- > 11′ FOV
- ≤30" angular resolution.

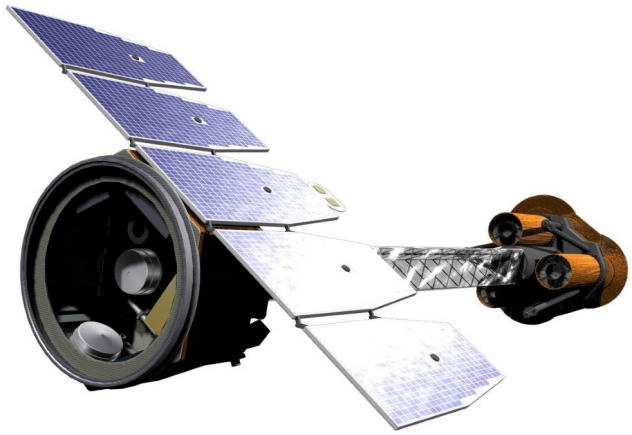

Figure 1. A concept drawing of IXPE as seen along the optical axis from left to right. The spacecraft (S/C) and its solar panels are on the left and the rear of the three telescopes assemblies are on the right. The overall length from aft of the S/C to the front of the optics is approximately 5-m.

3. THE POLARIZATION SENSITIVE DETECTORS

At the heart of each telescope system is a polarization-sensitive imaging detector that allows broad-band X-ray polarimetry with low net background and minimal, if any, systematic effects. These Gas Pixel Detectors (GPD), invented and developed by the Italian members of the team [13] and refined over the past 15 years to a high level of maturity, utilize the anisotropy of the emission direction of photoelectrons produced by polarized photons to gauge with high sensitivity the polarization state of X-rays interacting in a gaseous medium.

In photoelectric interactions — the dominant interaction process for X-rays in the *IXPE* energy range of 2–8 keV — the ejected K-shell photoelectron has an emission direction peaked around that of the electric field of the photon with a $\cos^2$ distribution. Thus, for polarized X-rays, all photoelectrons are preferentially emitted in the polarization direction. After ejection, each photoelectron interacts with the surrounding gas and is slowed by ionizing collisions and scattered by nuclei until it eventually stops. The resulting string of ionization, or photoelectron "track", marks the path of the photoelectron from its creation at the original X-ray interaction site to its stopping point. It is in the initial part of this

track where the information on the original electron direction is recorded. The distribution of these directions for many detected tracks then determines both the degree of polarization and the position angle associated with the incident photon beam.

The operation of the GPD is shown schematically in Figure 2. An incident X-ray photon enters through a thin gas-containment window and interacts in the detector fill gas, a mixture of low-Z components designed to maximize track length and to minimize diffusion (spreading of the track) while the signal is being collected. The ionization track, in turn, drifts towards a Gas Electron Multiplier (GEM). Here, each electron is multiplied to improve signal to noise, and the charge is transferred to a very-fine-pixel anode array for readout.

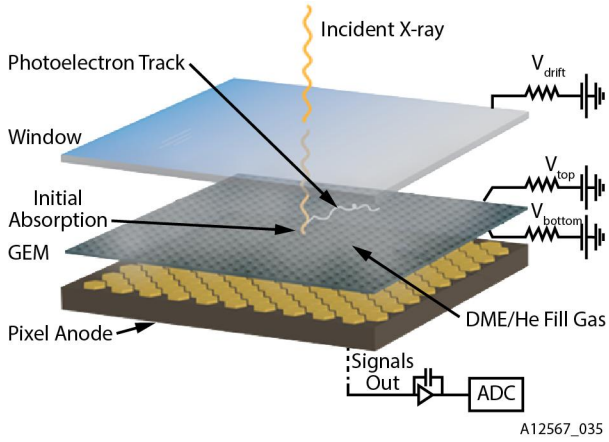

Figure 2. Schematic of the gas pixel detector.

The pixel anode readout [14], a CMOS-based Application Specific Integrated Circuit (ASIC), combines the functions of charge collection and readout electronics. This chip, now in its third generation, has a matrix (~100,000) of 50-μm hexagonal pixels each connected to a full electronic analog readout chain. A low system noise, combined with an effective GEM amplification of just 500, gives the ability to easily resolve individual electrons in the photoelectron track.

A typical track in He + DME (20/80), 1 cm depth and 1 atm pressure, is shown in Figure 3 to illustrate key features. The challenge in extracting the desired information arises from the fact that most of the signal is at the end of the track, whereas information on the photoelectron emission direction is at the less-intense beginning. The *IXPE* team has developed sophisticated and experimentally verified software that reliably determines the initial interaction point and the initial emission direction [15]. The best sensitivity to polarization is achieved by removing 20% of the tracks (those that contain less information about the initial photoelectron direction) and this is accounted for in all sensitivity calculations. The effective spatial resolution of the detector is accurate, on average, to 120 μm HEW (6″) across the full 2–8 keV band and better than 100 μm (5″) at 4.5 keV [16]. This spatial resolution is included in the system angular resolution budget as are the parallax effect of absorption depth within the detector. The latter arises because the cone of X-rays arriving from the optics comes to a focus at a point in the detector sensitive volume and then diverges again. As the detector has finite depth, some X-rays are stopped before they reach focus and others are stopped beyond this point. This effect creates an additional smearing of the initial interaction site, which has been modeled and accounted for in the angular resolution budget.

The measured detector energy resolution is typical of a proportional counter, 23% FWHM at 2.6 keV, scaling as $(1/\text{Energy})^{1/2}$. The detector sensitive area, 15×15 mm^2, defines the maximum instrument field of view, 12.8′×12.8′.

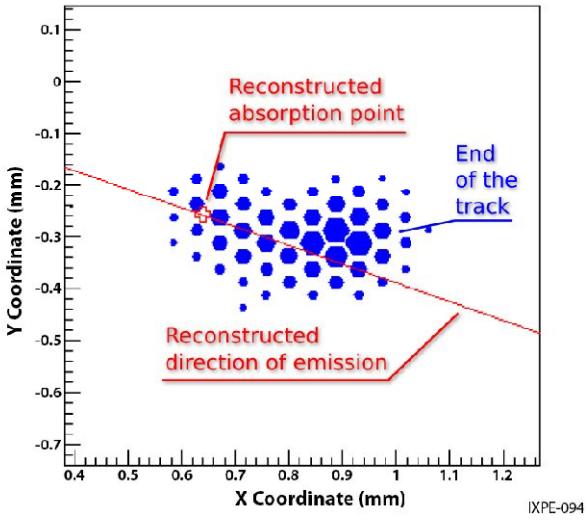

Figure 3. A GPD image of an electron track at 3.7 keV showing the absorption point, the end of the track, and the initial track direction.

A key factor in determining the sensitivity of the polarimeter is the modulation factor (μ), a measure of the variation of the measured track direction for a 100% polarized input. The modulation factor has been calibrated for the *IXPE* detectors at various X-ray energies. For energies between those measured, a sophisticated Monte-Carlo simulation has been developed and experimentally verified to aid in interpolation. Figure 4 shows measured and simulated data.

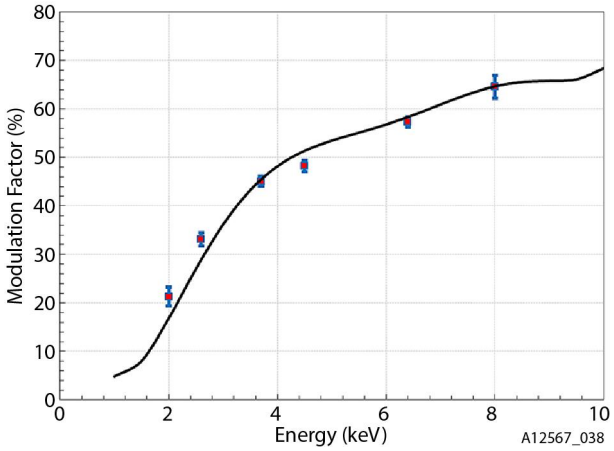

Figure 4. Measured modulation factor (data points) and results of a simulation (solid line) as a function of energy.

Equally important for any polarimeter is to show a lack of modulation for an unpolarized input signal. The *IXPE* detector has been extensively irradiated with unpolarized beams. For example, an unpolarized 5.9-keV beam, give residual modulation = 0.0018 ±0.0014. This is consistent with zero within the (3σ) uncertainty and shows that there is no evidence for any systematic effects at well under the 1% level. This is not surprising as the design of the 2-d readout is symmetric under rotation and only utilizes one technique for measuring the polarization direction. It should be noted that the 120º clocking of each telescope (Mirror Module Assembly + Detector Unit) with respect to the others, and the capability to periodically change the roll of the spacecraft (within solar-panel constraints) during an observation to rotate the detectors relative to the sky, would also enable residual spurious modulation to be removed from the data.

4. THE X-RAY TELESCOPES

The *IXPE* telescopes are full-shell Wolter-1 prescriptions[17], fabricated using an electroformed-nickel-cobalt replication process that has been developed and refined at MSFC since the early 1990s. MSFC will fabricate three flight mirror assemblies plus one spare comprising a total of 96 mirror shells. Each mirror assembly provides ~ 250 cm^2 effective area in the 3-6 keV band, MSFC has fabricated well over 500 thin-wall shells as part of a number of flight projects—including 224 replicated mirror shells fabricated, calibrated, environmentally tested and delivered for eight (seven flight plus one spare) individual telescopes for the Russian-led *ART-XC* instrument aboard the *Spectrum-Röntgen-Gamma* mission [18], 55 shells for the *FOXSI-2* rocket payload [19], and >100 shells for MSFC's High-Energy Replicated Optics (*HERO*) balloon payload [20],[21]. Figure 5 shows an example telescope.

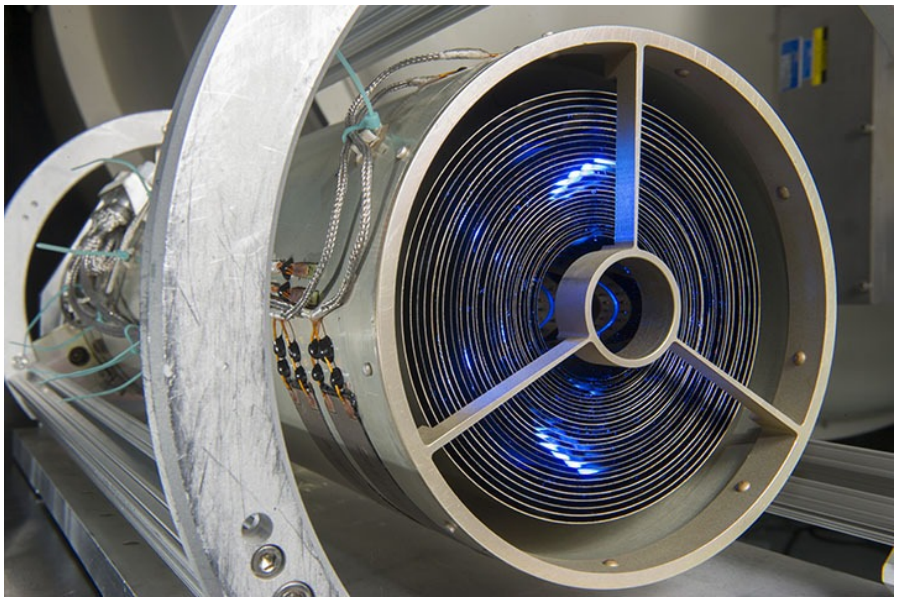

Figure 5. Photograph of one of the 8 ART-XC optics which are very similar to what is being planned for *IXPE*.

5. SCIENCE EXAMPLES EMPHASIZING THE BENEFITS OF IMAGING.

This section we demonstrates the scientific power of *IXPE*, concentrating on but a few of the paradigm-changing observations that may be conducted with the Observatory. For a full flavor of the science that may be accomplished with IXPE (and its European cousin XIPE), refer to the recent symposium held in Valencia, Spain May 24-26, 2016 [2].

With its imaging capabilities, *IXPE* can obtain scientifically meaningful polarimetric images of the brightest extended X-ray sources: Active Galactic Nucleus (AGN) jets, Pulsar Wind Nebulae (PWNe), and (shell-type) Supernova Remnants (SNR). Position- and energy-dependent polarization maps of such synchrotron emitting sources will elucidate the magnetic-field structure of the X-ray emitting regions, which may differ from those of regions emitting in other spectral bands (radio or visible, where available). As radiative lifetimes for X-ray-emitting electrons are much shorter than those of electrons radiating at lower energies, X-ray polarimetric imaging better indicates the magnetic structure in regions of strong electron acceleration.

Besides mapping the X-ray polarization of several extended sources, *IXPE* imaging capabilities avoids source confusion by resolving point sources from surrounding nebular emission or from adjacent point sources. In the absence of good angular resolution, polarization measurements of individual sources in a confused region are impossible without other information—e.g., phase-resolved flux of a pulsed source. Even in those cases where a pulsed point source can be isolated from a steady extended source using phase-resolved data, the statistical noise due to the extended source cannot

[2] http://www.isdc.unige.ch/xipe/index.php/first-xipe-science-meeting

be removed. Thus, imaging provides a more sensitive polarization measurement of the target point source than a non-imaging system with comparable sensitivity for isolated point sources.

Figure 6 displays the simulated *IXPE* image and polarization-error contour maps of the jet in the AGN Centaurus A (Cen A), after subtraction of a diffuse, azimuthally symmetric central component. The polarization model assumes that the jet's magnetic field is axial in low-intensity regions and transverse in high-intensity regions, as might occur in a shock. Note the two serendipitous X-ray sources within 3′ (ESE and SW) of the center of Cen A. *IXPE* easily resolves these relatively bright, possible Ultra-Luminous X-ray (ULX) sources from the Cen-A synchrotron core thus avoiding source confusion and providing additional data.

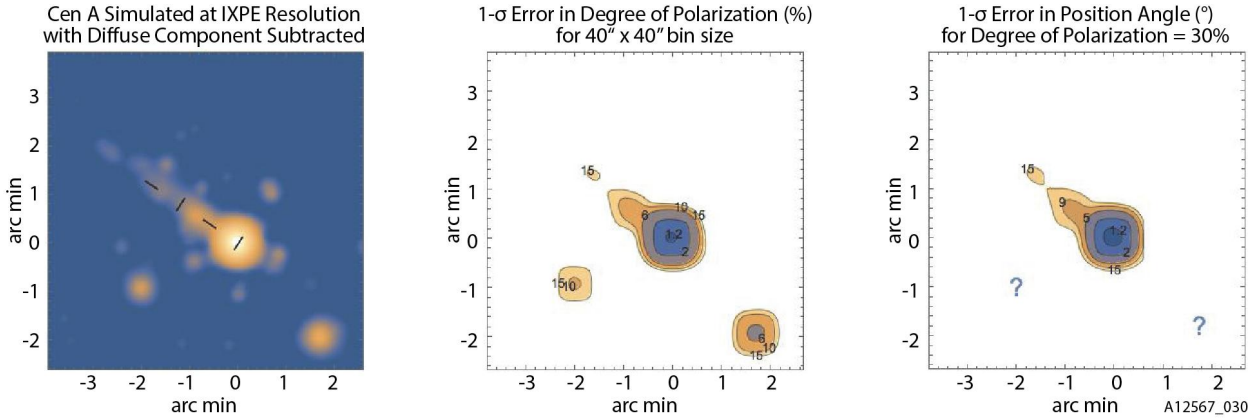

Figure 6. Simulated IXPE polarimetric imaging of the jet in the AGN Cen A. Left panel shows the intensity image with superposed polarization model; center, contour map of the polarization statistical error in polarization degree; and right, contour map of the uncertainty in the position angle. Errors are for 40″×40″ bins and a long but achievable exposure.

Figure 7 displays the simulated *IXPE* image and polarization-error contour maps of the Crab PWNe, after adding a point source to synthesize the phase-average pulsar. The polarization model assumes that the X-ray polarization field is the same as that in the visible band.[22]

In addition to mapping polarization of extended sources, *IXPE* imaging capabilities enable more sensitive measurements of the polarization properties of point sources embedded in nebular emission or adjacent to other sources. Note that, *even if the contributions of the unresolved sources can be modeled*—e.g., using phase resolved data for a pulsed source—the statistical noise from the confusing sources still adversely affects measurement of the polarization properties of the intended target. These confusing sources essentially constitute a background, which—depending upon the relative contributions of the sources and the imaging resolution of the polarimeter—could be significant with respect to the source counts!

A prominent example of this circumstance is a pulsar within its PWNe—e.g., the Crab pulsar and Nebula. The phase-average X-ray flux of the Crab pulsar is only about 0.08 that of its PWNe, which has an approximate diameter of 90″ = 1.5′. As *IXPE*'s angular resolution (30″ = 0.5′ Half Power Diameter) partially resolves the PWNe, this imaging capability *improves the sensitivity for measuring X-ray polarization of the pulsar* by reducing the contribution of the resolved PWNe to the "background" counts. Figure 8 blue curve) displays the polarizarion measurement error at the 99%-confidence level for the phase-average pulsar as a function of the radius of a measurement aperture centered on the pulsar, using the simulated *IXPE* image in Figure 7. For the optimal aperture radius (15″ ≈ HPD/2), the MDP is 1.7 times lower (more sensitive) than for a measurement with no angular resolution (red line). This means that *IXPE* can measure the phase-average polarization of the Crab pulsar (embedded in its PWNe) to a given sensitivity in about $1/3 = (1/1.7)^2$ the time required for a non-imaging polarimeter having an identical polarization sensitivity for an *isolated* point source.

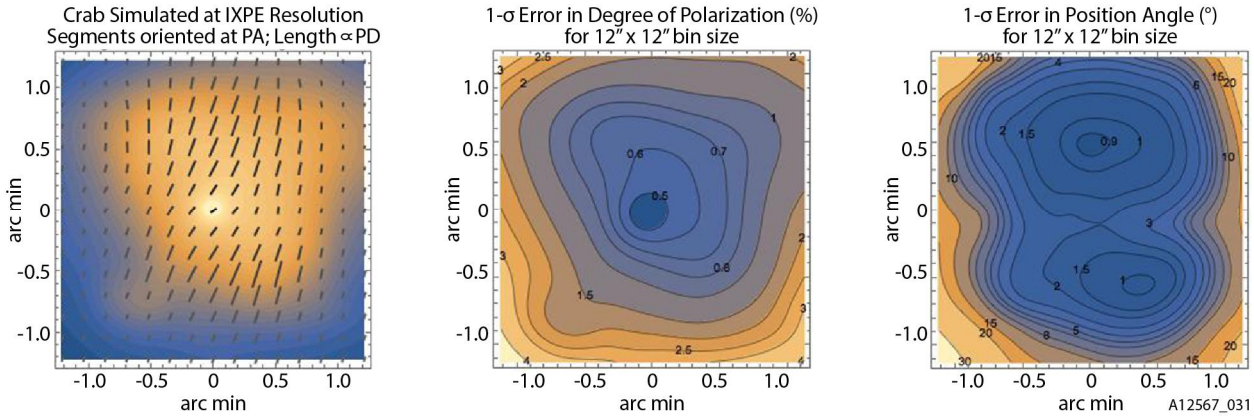

Figure 7. Simulated *IXPE* polarimetric imaging of the Crab PWNe and pulsar. Left panel shows the intensity image with superposed polarization model; center, contour map of the uncertainty in the degree of polarization; and right, contour map of the degree of uncertainty in the position angle. Computed errors are for 12″×12″ bins and a short exposure.

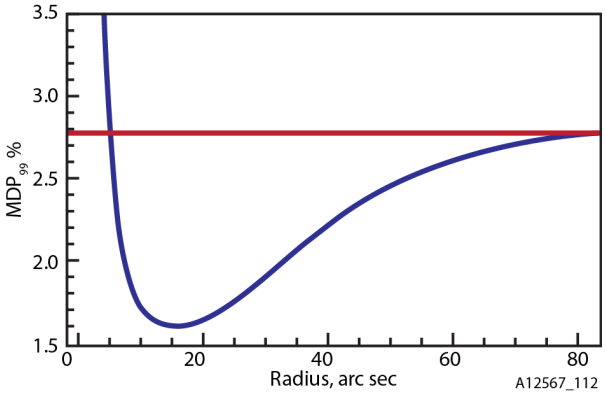

Figure 8. MDP_{99} for the (phase-average) emission of the Crab pulsar, based upon a simulation of a short *IXPE* observation of the Crab pulsar and its PWNe. The blue curve gives the dependence of MDP_{99} upon aperture radius for an *IXPE* image; the red line is the MDP for a non-imaging polarimeter (with the same sensitivity for isolated point sources as *IXPE*)

Figure 8 displays the simulated *IXPE* image and polarization-error contour maps of the PWNe MSH 15-52 and pulsar B1598-58. The polarization model assumes strong polarization in the southeast jet, with position angle corresponding to an axial magnetic field, and weaker polarization elsewhere.

Figure 9 displays the simulated *IXPE* image and polarization-error contour maps of the bright SNR Cassiopeia A (Cas A). The image is based upon ACIS data filtered by hardness ratio to pass primarily non-thermal emission. The polarization model is based upon radio polarization maps of Cas A, which indicate a radial magnetic field at the radio rim of the SNR.[23] Note, however, that the X-ray shell—which best marks the acceleration region—lies outside the radio rim and thus might display different magnetic structure.

Figure 10 displays the simulated *IXPE* image and polarization-error contour maps of the SNR Tycho. The image is based upon ACIS data filtered by hardness ratio to pass primarily non-thermal emission. The polarization model is guided by radio polarization maps of SNRs.[24]

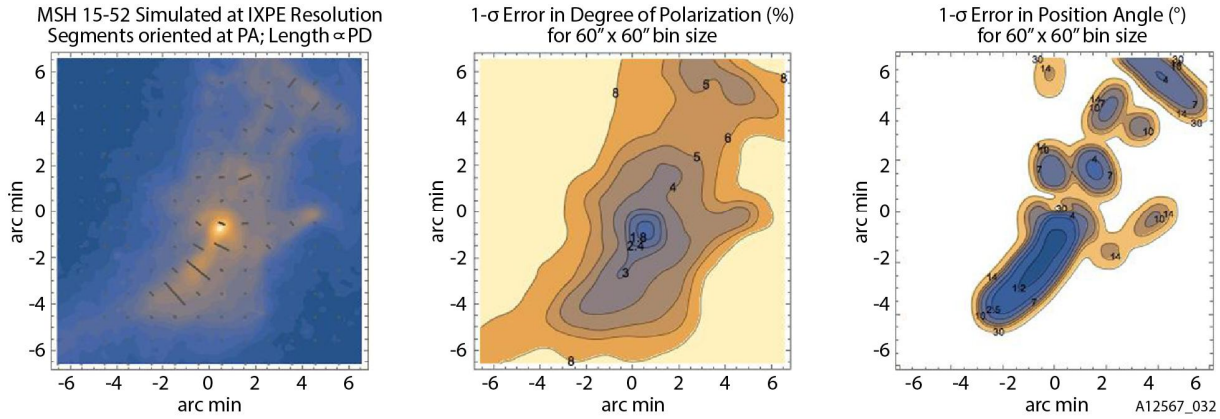

Figure 9. Simulated IXPE polarimetric imaging of the PWNe MSH 15-52 and pulsar B1598-58. Left panel shows the intensity image with superposed polarization model; center, contour map of the uncertainty in the degree of polarization; and right, contour map of the uncertainty in the position angle. Computed errors are for 60″×60″ bins and a long exposure.

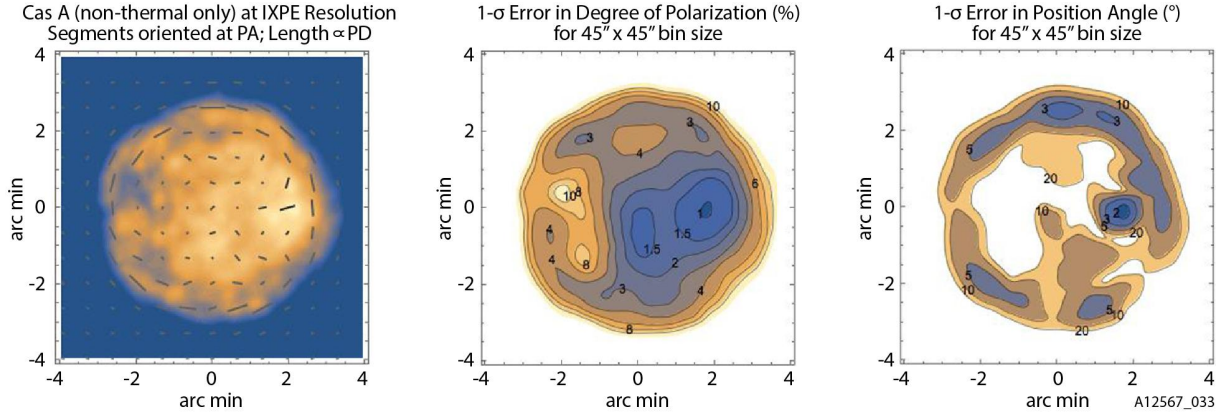

Figure 10. Simulated IXPE polarimetric imaging of the SNR Cas A. Left panel shows the intensity image with superposed polarization model; center, contour map of the uncertainty in the degree of polarization; and right, contour map of the degree of uncertainty in the position angle. Computed errors are for 45″×45″ bins and a long but achievable exposure.

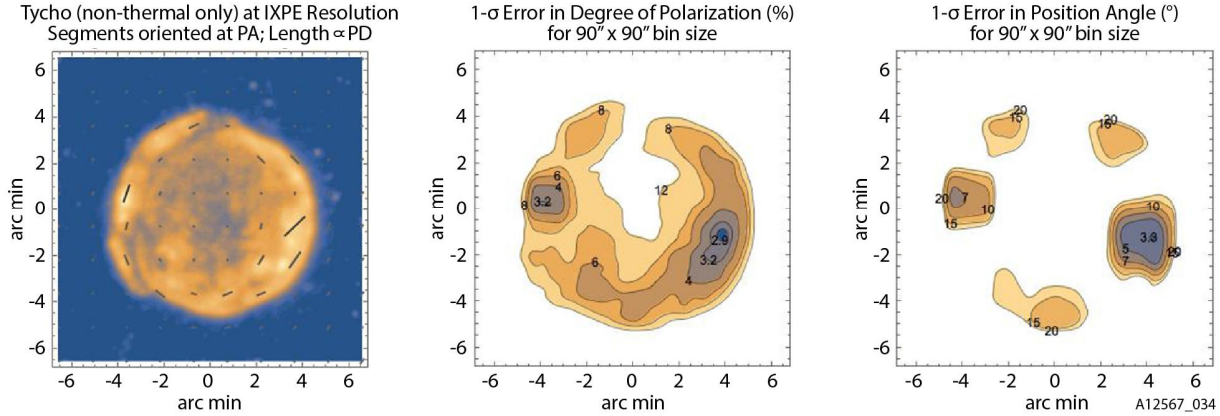

Figure 11. Simulated IXPE polarimetric imaging of the SNR Tycho. Left panel shows the intensity image with superposed polarization model; center, contour map of the uncertainties in the degree of polarization; and right, contour map of the uncertainties in the position angle. Computed errors are for 90″×90″ bins and a long exposure.

6. CONCLUSIONS

The *IXPE* is a bold new instrument with proven technology that can open new frontiers in X-ray Astronomy. By adding polarization measurements to the arsenal of observational techniques, X-ray polarimetry can provide new insights into a myriad of astrophysical settings where physical asymmetries such as magnetic fields, scattering from aspherical geometries, etc. predominate. IXPE exploits polarimetric imaging to map some of the brightest extended X-ray sources, reduce source confusion and enhance sensitivity in those cases where for point sources embedded in diffuse sources. Because of the imaging capability we know of no rival instrument that exceeds its capabilities.

7. ACKNOWLEDGEMENTS

Besides the authors of this article, many more have contributed to the development of the instrumentation and to the science case for the mission. These include N. Bucciantini, E. Churazov, M. Dovciak, R. Goosmann, S. Gunji, V. Karas, F. Marin, G. Pavlov, P. Petrucci, J. Poutanen, M. Salvati, L. Stella, R. Sunyaev, R. Taverna, K. Wu, and S. Zane.

REFERENCES

[1] Novick, R., Weisskopf, M. C., Berthelsdorf, R., Linke, R., & Wolff, R. S., "Detection of X-Ray Polarization of the Crab Nebula", ApJ, 174, L1 (1972).
[2] Weisskopf, M. C., Cohen, C. G., Kestenbaum, H. L., Long, K. S., Novick, R., & Wolff, R. S., "Measurement of the X-ray polarization of the Crab Nebula", ApJ, 208, L125 (1976).
[3] Weisskopf, M. C., Silver, E. H., Kestenbaum, H. L., Long, K. S., Novick, R., "A precision measurement of the X-ray polarization of the Crab Nebula without pulsar contamination", ApJ, 220, L117 (1978).
[4] Silver, E. H., Weisskopf, M. C., Kestenbaum, H. L., Long, K. S., Novick, R., & Wolff, R. S., "The first search for X-ray polarization in the Centaurus X-3 and Hercules X-1 pulsars", ApJ, 232, 24 (1979)
[5] Weisskopf, M. C., Kestenbaum, H. L., Long, K. S., Novick, R., & Silver, E. H., "An upper limit to the linear X-ray polarization of Scorpius X-1", ApJ, 221, L13 (1978).
[6] Winkler, C., Diehl, R., Ubertini, P., & Wilms, J.," INTEGRAL: Science Highlights and Future Prospects", SSRv, 161, 149 (2011).
[7] Chauvin, M., Roques, J. P., Clark, D. J., & Jourdain, E., "Polarimetry in the Hard X-Ray Domain with INTEGRAL SPI", ApJ, 769, 137 (2013).
[8] Forot, M., Laurent, P., Grenier, I. A., Gouiffès, C., & Lebrun, F., "Polarization of the Crab Pulsar and Nebula as Observed by the INTEGRAL/IBIS Telescope", ApJ, 688, L29 (2008).
[9] Jourdain, E., Roques, J. P., Chauvin, M., & Clark, D. J., "Separation of Two Contributions to the High Energy Emission of Cygnus X-1: Polarization Measurements with INTEGRAL SPI ", ApJ, 761, 27 (2012).
[10] Ubertini, P., Corsi, A., Foley, S., McGlynn, S., De Cesare, G., & Bazzano, A., "The INTEGRAL view of Gamma-Ray Bursts ", AdSpR, 47, 1374 (2011).
[11] Götz, D., Covino, S., Fernández-Soto, A., Laurent, P., & Bošnjak, Ž., "The polarized gamma-ray burst GRB 061122 ", MNRAS, 431, 3550 (2013).
[12] Götz, D., Laurent, P., Antier, S., Covino, S., D'Avanzo, P., D'Elia, V., & Melandri, A., "GRB 140206A: the most distant polarized gamma-ray burst", MNRAS, 444, 2776 (2014).
[13] Costa, E., Soffitta, P., Bellazzini, R., Brez, A., Lumb, N. Spandre, G., Nature, "An efficient photoelectric X-ray polarimeter for the study of black holes and neutron stars ", Vol 411, 662 (2001).
[14] Bellazzini, R., Spandre, G., Minuti, M., Baldini, L., Brez, A. et al., "Direct reading of charge multipliers with a self-triggering CMOS analog chip with 105 k pixels at 50 mum pitch", Nucl. Instr. & Meth. A566, 552 (2006).
[15] Bellazzini, R., Angelini, F., Baldini, L., Brez, A., Costa, E., et al.," Novel gaseus X-ray polarimeter: data analysis and simulation", SPIE 4843, 383 (2003).
[16] Soffitta, P., Muleri, F., Fabiani, S., Costa, E., Bellazzini, R., et al., "Measurement of the position resolution of the Gas Pixel Detector", NIMPA, 700, 99 (2013).
[17] Wolter, H.," Spiegelsysteme streifenden Einfalls als abbildende Optiken für Röntgenstrahlen", Ann. Phys. 445, 94. 1952,

[18] Gubarev, M., Ramsey, B., Kolodziejczak, J. J., O'Dell, S. L., Elsner, R., et al.," The calibration of flight mirror modules for the ART-XC instrument on board the SRG mission", Proc. SPIE, 9144, 6 (2014).
[19] Krucker, S., Christe, S., Glesener, L., Ishikawa, S., et al., "First Images from the Focusing Optics X-Ray Solar Imager",ApJ, 793, issue 2, L32 (2014).
[20] Ramsey, B. D. ," The development of focusing optics for the hard-X-ray region", Advances in Space Research, 38, Issue 12, 2985 (2006).
[21] Ramsey, B. D., Elsner, R. F., Engelhaupt, D. E., O'Dell, S. L., Speegle, C. O. et al, "Development of hard x-ray optics at MSFC", SPIE, 4851, 631 (2003).
[22] Moran, P., Shearer, A., Mignani, R. P., Słowikowska, A., De Luca, A., et al., "Optical polarimetry of the inner Crab nebula and pulsar", MNRAS, 433, 2564 (2013).
[23] Anderson, M. C., Keohane, J. W., & Rudnick, L., "The polarization and depolarization of radio emission from supernova remnant Cassiopeia A", ApJ, 441, 300 (1995).
[24] Dubner, G., & Giacani, E., "Radio emission from supernova remnants ", A&ARv, 23, 3 (2015).